© 2023. Published by The Company of Biologists Ltd | Development (2023) 150, dev201405. doi:10.1242/dev.201405

STEM CELLS AND REGENERATION

RESEARCH REPORT

Cyclin A participates in the *TSO1-MYB3R1* regulatory module to maintain shoot meristem size and fertility in *Arabidopsis*

Fuxi Wang, Wanpeng Wang* and Zhongchi Liu‡

ABSTRACT

The stem cell pools at the shoot apex and root tip give rise to all the above- and below-ground tissues of a plant. Previous studies in *Arabidopsis* identified a *TSO1-MYB3R1* transcriptional module that controls the number and size of the stem cell pools at the shoot apex and root tip. As TSO1 and MYB3R1 are homologous to components of an animal cell cycle regulatory complex, DREAM, *Arabidopsis* mutants of *TSO1* and *MYB3R1* provide valuable tools for investigations into the link between cell cycle regulation and stem cell maintenance in plants. In this study, an *Arabidopsis* cyclin A gene, *CYCA3;4*, was identified as a member of the *TSO1-MYB3R1* regulatory module and *cyca3;4* mutations suppressed the *tso1-1* mutant phenotype specifically in the shoot. The work reveals how the *TSO1-MYB3R1* module is integrated with the cell cycle machinery to control cell division at the shoot meristem.

KEY WORDS: Cell cycle, Cyclin A, DREAM complex, MYB3R1, Shoot meristem, TSO1

INTRODUCTION

Plant meristems are responsible for generating all above and below ground tissues. The identification of gene regulatory circuitries that confer and maintain the 'stem cell' property in plant meristems is therefore of fundamental importance. In plant shoot apical meristem (SAM), the *WUSCHEL (WUS)-CLAVATA (CLV)* negative-feedback loop maintains the stem cell pool and limits the meristem size. However, beyond the *WUS-CLV3* pathway, there have been limited studies of other regulatory pathways for SAM regulation, and little is known about how the plant meristem activities are integrated with the cell cycle regulation.

The DREAM/MMB complex is a master cell cycle regulator in both animals and plants (Kobayashi et al., 2015; Sadasivam and DeCaprio, 2013). The animal DREAM complex consists of retinoblastoma (RB)-like proteins (P107 and P130), E2Fs and their dimerization partners DP1-3 and the MuvB core (LIN9, LIN37, LIN52, LIN54 and RBBP4). In animal quiescent cells, the DREAM complex prevents cells from entering the cell cycle while in dividing cells, the MuvB core associates with B-Myb (also called MYBL2) instead of the Rb-like proteins to form the MMB complex that promotes the G2/M phase (Fischer and Müller, 2017). Recent studies revealed that the DREAM/MMB complexes also exist in plants. The *Arabidopsis* genome possesses essentially all the homologous genes of the DREAM/MMB complex components, and the corresponding plant homologs can form similar complexes (Lang et al., 2021; Ning et al., 2020). Intriguingly, plants have more copies of each complex component. For example, there are eight *Arabidopsis* homologs of LIN54, named as *TSO1*, *SOL1*, *SOL2*, *TCX4*, *TCX5*, *TCX6*, *TCX7* and *TCX8*, all of which encode two cysteine-rich CXC motifs separated by a linker region (Andersen et al., 2007; Hauser et al., 2000; Song et al., 2000). TCX5/6-containing DREAM complexes in *Arabidopsis* act to preclude DNA hypermethylation and prevent excessive cell proliferation (Ning et al., 2020), and the *Arabidopsis SOL1* and *SOL2* are required for efficient cell fate transitions in the stomata lineage (Simmons et al., 2019). The existence of multiple paralogs in plant genomes could contribute to different isoforms of the DREAM/MMB complex acting in different developmental contexts.

In animals, disruptions of the DREAM/MMB complex usually lead to cancer. The loss of both retinoblastoma protein (pRb) and Rb-like (p107/p130) induces retinoblastoma in mice (Wu et al., 2017), while overexpression of B-Myb is found in many cancers, including breast cancer and colorectal cancer, and is often associated with poor outcomes (Musa et al., 2017). Although plants do not suffer from cancer, plant mutants defective in the DREAM/MMB components exhibit shoot meristem fasciation: an over-proliferation of the SAM. In *Arabidopsis*, the *tso1-1*, an antimorphic mutation in the *Arabidopsis* homolog of LIN54, shows fasciated SAMs, and *tso1-1* mutant flowers fail to differentiate into floral organs, and are therefore sterile (Liu et al., 1997; Sijacic et al., 2011; Wang et al., 2018). Meanwhile, the cells in the *tso1-1* root apical meristem (RAM) exit the cell cycle early, resulting in a short root phenotype, suggesting *TSO1* has different and opposite effects on shoot and root meristems. *tso1-3*, a loss-of-function allele, on the other hand, has weak phenotypes; it develops normal flowers and normal length root but exhibits reduced fertility (Hauser et al., 2000; Sijacic et al., 2011; Wang et al., 2018). In *Arabidopsis*, *SOL2* is highly similar to *TSO1*, not only in sequence but also in expression; *tso1-3; sol2-1* double loss-of-function mutants exhibit a synergistic genetic interaction and a *tso1-1*-like phenotype. Therefore, the *tso1-1* antimorphic allele may inactivate *TSO1* as well as *SOL2* to cause its severe phenotype (Sijacic et al., 2011). These different alleles of *TSO1* in *Arabidopsis* provide a useful tool for dissecting DREAM/MMB function in the context of plant meristem regulation.

To identify genes that may act in the same pathway as *TSO1*, we previously conducted a genetic screen for suppressors of *tso1-1* (Wang et al., 2018). Seeds of *tso1-1* containing an inducible *TSO1* (*35S::TSO1-GR*) were mutagenized. When applied with dexamethasone (DEX), *tso1-1; 35S::TSO1-GR* M1 plants were able to overcome sterility and gave rise to M2 progeny, which were screened for suppressors. Thirty-two suppressors from the screen were found to reside in *MYB3R1*, which encodes one of the five

Department of Cell Biology and Molecular Genetics, University of Maryland, College Park, MD 20742, USA.
*Present address: Cardiovascular Research Institute, University of California, San Francisco, CA 94143, USA.

‡Author for correspondence (zliu@umd.edu)

F.W., 0000-0002-2873-7165; Z.L., 0000-0001-9969-9381

Handling Editor: Ykä Helariutta
Received 27 October 2022; Accepted 6 February 2023

Development (2023) 150, dev201405. doi:10.1242/dev.201405

Arabidopsis homologs of B-Myb. The work established that the wild-type *TSO1* activity is required to repress *MYB3R1* expression to prevent SAM overproliferation (Wang et al., 2018). However, questions concerning how the *TSO1-MYB3R1* module regulates SAM cell proliferation and how the module interacts with cell cycle machinery remain unanswered.

In this study, we characterized a second suppressor locus of *tso1-1* from the same genetic screen. We showed that mutations in an A-type cyclin named *CYCA3;4* suppressed the abnormal floral organ development, shoot fasciation and sterility of *tso1-1* to certain degrees. Additionally, ectopic and more abundant CYCA3;4-GUS proteins were found in *tso1-1* mutant inflorescence, and *CYCA3;4* overexpression enhanced the *tso1-3* phenotype. The work reveals the function of a specific cyclin A in shoot meristem regulation and directly integrates cell cycle machinery with the *TSO1-MYB3R1* regulatory module.

RESULTS AND DISCUSSION

A splice-site mutation in *CYCA3;4* suppresses the *tso1-1* shoot phenotype

In order to identify new components of the *TSO1* regulatory pathway, a second suppressor locus, defined by a single allele, *A144*, was analyzed. *A144* suppresses *tso1-1* defects in floral organ differentiation, fertility and shoot meristem size (Fig. 1A). Although *tso1-1* plants develop highly abnormal carpels (Fig. 1A) that lead to no seeds per carpel (Fig. 1B), *tso1-1; A144* double plants form normal carpels (Fig. 1A) that yield 1-10 seeds per silique (Fig. 1B). Furthermore, 100% *tso1-1* mutant shoot meristems are fascinated (Fig. 1B), as shown by more floral buds per inflorescence (Fig. 1A). This meristem fasciation defect of *tso1-1* is completely suppressed in *tso1-1; A144* double mutants (Fig. 1A,B). In the weaker allele of *tso1-3*, even though the carpels develop properly, their fertilities are low, which is indicated by the small siliques; however, *tso1-3; A144*

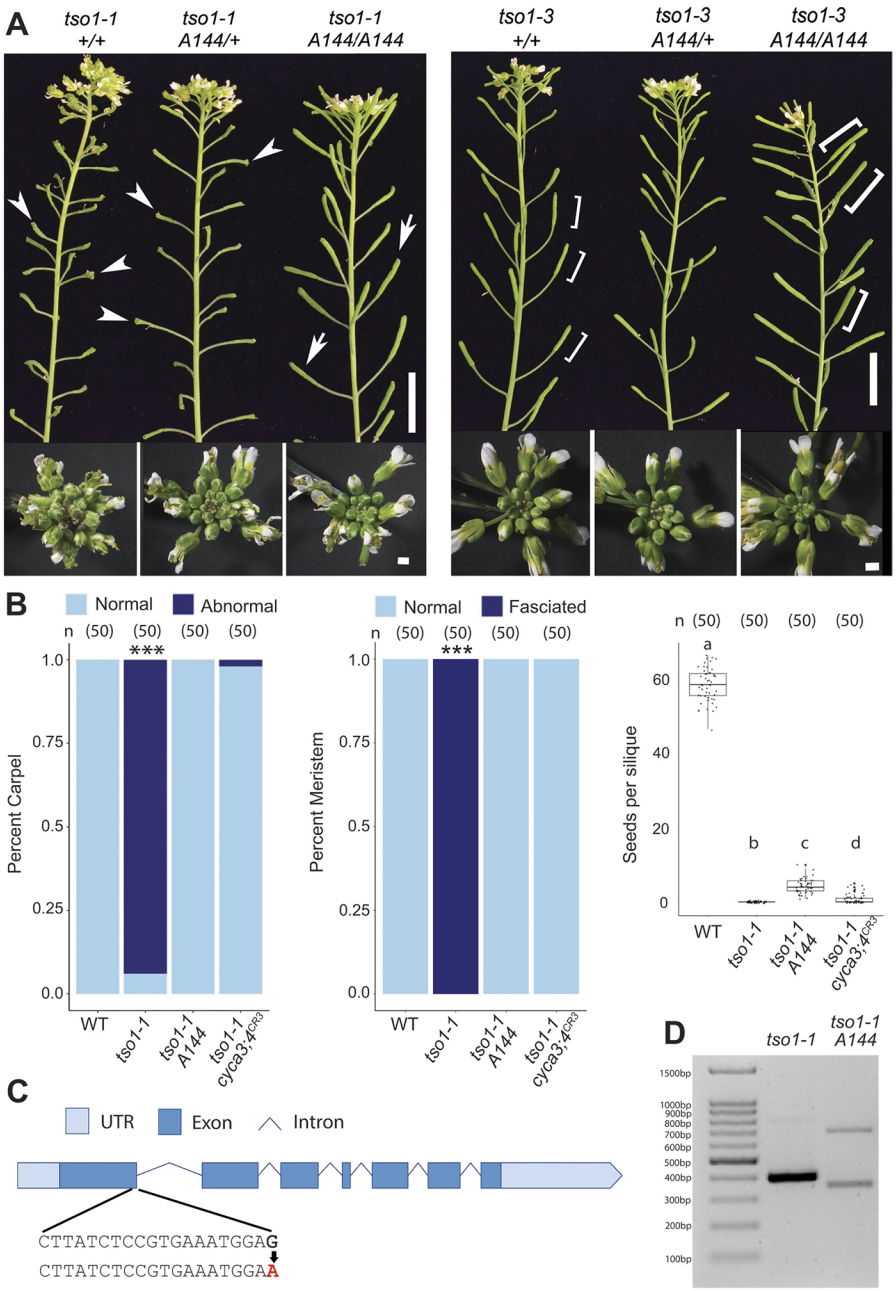

Fig. 1. A homozygous *A144* mutation suppresses defects of *tso1-1* and *tso1-3*. (A) Comparison of inflorescences and siliques among *tso1-1* and *tso1-3* plants heterozygous or homozygous for the *A144* mutation. The top panel illustrates carpel phenotype and silique length. Arrowheads indicate abnormal carpels; arrows indicate fertile siliques. The bottom panel illustrates shoot meristems. All plants containing *tso1-1* also possess the *35S::TSO1-GR* transgene but are not treated with dexamethasone (DEX). *tso1-3* has a weaker defect in fertility (top panel) and a normal SAM (bottom). Homozygous *A144* improves *tso1-3* fertility with longer and fuller siliques (indicated by bracket size). Scale bars: 1 cm (upper panel); 1 mm (lower panel). (B) Quantification of abnormal carpels, meristem fasciation and seeds per silique in different genotypes. The number of carpels, meristems and siliques is indicated in parenthesis. ***P<0.001 compared with other genotypes (unpaired, two-tailed t-test). a-d indicate significance differences in each comparison (P<0.001; unpaired, two-tailed t-test). In the box plot, the horizontal lines indicate the medians, and the whiskers indicate maximum and minimum values. *cyca3;4*^{CR3} is a CRISPR-edited new allele of *CYCA3;4* detailed in Fig. 2. (C) Gene model of *CYCA3;4*. The G-to-A mutation is highlighted in red. (D) RT-PCR showing two aberrant transcripts in *tso1-1; A144* double mutants.

Development (2023) 150, dev201405. doi:10.1242/dev.201405

double mutants form longer siliques than *tso1-3* single mutants (Fig. 1A).

To isolate the gene defined by the *A144* suppressor, a F2 mapping population was created and sequenced. Using the SIMPLE mapping pipeline (Wachsman et al., 2017), *A144* was mapped to an A-type cyclin gene *CYCA3;4* on chromosome 1 (Fig. S1). A G-to-A mutation occurs in the last nucleotide of the first exon of *CYCA3;4* and is synonymous (E-to-E) (Fig. 1C). RT-PCR was used to examine whether this mutation affects the splicing of *CYCA3;4* transcripts. A *CYCA3;4* transcript of wild-type size was not detected in the *A144* plants, but two transcripts of aberrant sizes were detected (Fig. 1D). Sequence analysis of the RT-PCR products showed that the longer aberrant transcript retained the first intron whereas the shorter aberrant transcript used a cryptic splice donor site in the first exon. As both the aberrant transcripts contained premature stop codons, *A144* likely caused a non-functional *CYCA3;4*.

CRISPR/Cas9-mediated knockouts of *CYCA3;4* also suppress *tso1-1*

To confirm that the mutated *CYCA3;4* is indeed the causal mutation for *A144*, we conducted both complementation tests and CRISPR/Cas9 knockout of *CYCA3;4*. The genomic sequence of *CYCA3;4* (*gCYCA3;4;* from ∼1.4 kb upstream to the end of 3'UTR) was transformed into the *A144* plants containing the *tso1-1* mutation. If the transgene rescues *A144*, the resulting transgenic plants should regain the *tso1-1* mutant phenotype, which was indeed observed, including meristem fasciation and complete sterility (Fig. S2). Second, a CRISPR/Cas9 construct with a gRNA targeting the first exon of *CYCA3;4* was transformed into *tso1-1; 35S::TSO1-GR* plants. Several T_1 plants showed suppressed phenotypes even in the absence of DEX application (Fig. 2A). Sequencing of the *CYCA3;4* locus in these T1 plants showed either homozygous or biallelic mutations in *CYCA3;4* (Fig. 2E). Detailed characterization of a *tso1-1; cyca3;4*^{CR3} homozygous line showed that these mutant plants formed normal shoots and carpels, and developed somewhat elongated siliques containing 0-5 seeds per silique (Fig. 2A,B; Fig. 1B). Therefore, CRISPR-mediated knockouts of *CYAC3;4* also suppress *tso1-1*, although the suppression of fertility, like *A144*, is incomplete. Together, these data strongly support that, in addition to *MYB3R1*, *CYCA3;4* defines a second suppressor locus of *tso1-1*.

CRISPR/Cas9-directed knockout of *CYCA3;4* allowed us to investigate whether the *cyca3;4* mutations could suppress the *tso1-1* short root phenotype without worries of background mutations caused by the EMS mutagenesis. Both *tso1-1* and *tso1-1; cyca3;4*^{CR3} plants had similar root length, which is shorter than that of wild-type L*er* (Fig. 2C,D), suggesting that mutations in *CYCA3;4* do not suppress the short root phenotype of *tso1-1*. It remains to be determined whether this tissue-specific suppression of *tso1-1* by the *cyca3;4* mutation is due to tissue-specific function of different members of the *CYCA3* family.

Among the 50 putative cyclin genes in the genome, categorized into *CYCA1-3*, *CYCB1-3*, *CYCC*, *CYCD1-7*, *CYCH*, *CYCL*, *CYCP1-4* and *CYCT* classes (Menges et al., 2005), *CYCA3* genes are believed to govern the G1-S transition and hence resemble the E-type cyclin in animals (Yu et al., 2003). However, the expression profiles of the four *Arabidopsis CYCA3s* vary greatly, suggesting potentially diverse functions (Takahashi et al., 2010; Willems et al., 2020). *CYCA3;3 (AT1G47220)* is a meiosis-specific cyclin (Bulankova et al., 2013), and the transcripts of *CYCA3;1* (*AT5G43080*) and *CYCA3;2* (*AT1G47210*) peak in the G1/S phase (Takahashi et al., 2010). *CYCA3;4* (*AT1G47230*), on the other hand, has been shown to be expressed throughout the cell cycle based on RT-PCR analysis of aphidicolin synchronized cell lines (Takahashi et al., 2010). More recently, CYCA3;4-GUS protein accumulation was examined in synchronized root tip by hydroxyurea treatment and shown to accumulate prominently in the G2/M phase (Willems et al., 2020). A loss-of-function *cyca3;4-1*

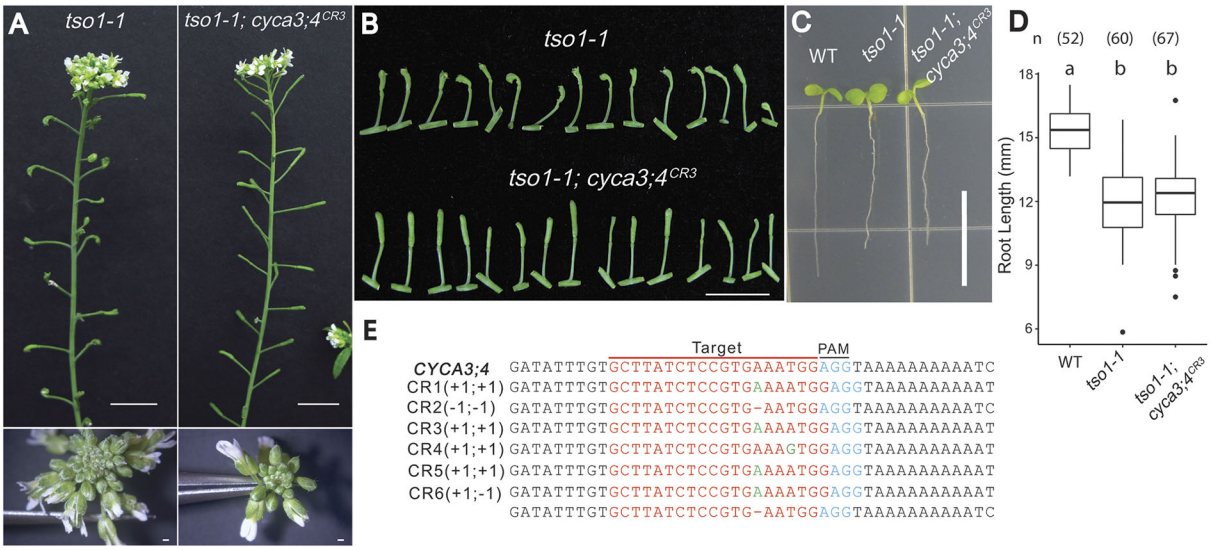

Fig. 2. CRISPR/Cas9 knockouts of *CYCA3;4* suppress *tso1-1* shoot but not root defects. (A) Defects of *tso1-1* in proper carpel development (top) and meristem fasciation (bottom) are suppressed by a CRISPR knockout mutation in *CYCA3;4*. (B) A comparison of abnormal carpels of *tso1-1* with short siliques of *tso1-1; cyca3;4*^{CR3}. The abnormal *tso1-1* carpels could not be fertilized and contained no seed; the *tso1-1; cyca3;4*^{CR3} carpels were fertilized and formed short siliques with a few seeds inside. (C) *tso1-1* mutants develop short roots in comparison with wild type (L*er*). A *tso1-1; cyca3;4*^{CR3} double mutant has a root length similar to that of *tso1-1*. (D) Quantification of root length in different genotypes. The number of examined roots is indicated in parenthesis. A significant difference is indicated between a and b (P<0.001; one-way ANOVA and Tukey's test). The horizontal lines indicate the medians, and the whiskers indicate the maximum and minimum values. (E) CRISPR/CAS9-generated mutant alleles of *CYCA3;4*. Red font indicates the seed RNA; green font indicates insertions, – and + indicate deletion and insertion, respectively; blue font indicates the protospacer adjacent motif (PAM) . Scale bars: 1 cm in A (upper images), B and C; 500 µm in A (lower images).

Development (2023) 150, dev201405. doi:10.1242/dev.201405

was previously identified as a suppressor of *ccs52a-1*, and two T-DNA insertion lines (*cyca3;4-2* and *cyca3;4-3*) showed strong reductions of transcripts but no obvious root or shoot phenotype (Willems et al., 2020). *A144* is therefore named as *cyca3;4-4*.

CYCA3;4 is misregulated in *tso1-1* mutants

To understand the mechanism of *tso1* suppression by *cyca3;4*, we constructed and analyzed a translational reporter of *CYCA3;4* (*pCYCA3;4-gCYCA3;4-GUS*), where a 1.4 kb promoter plus the coding region of *CYCA3;4* was fused to *GUS*. The construct was transformed into plants heterozygous for *tso1-1*, and seven independent transgenic lines were analyzed. Reporter GUS expression was compared among the T_2 siblings from the same T_1 parent; these T_2 siblings are either *tso1-1* or wild type (+/+ or *tso1-1*/+). In the T_2 wild-type inflorescences, light and consistent blue staining was observed in the young floral buds (Fig. 3A,B). At floral stages 9-10, the locules of anthers show intense blue staining (white arrow in Fig. 3A); at stages 10-12, intense staining occurs in ovules inside the gynoecium as well as stigma (see inset of Fig. 3A). Therefore, the CYCA3;4 protein is at the highest level in actively dividing germ cells. In *tso1-1* mutant inflorescences, young floral buds showed significantly stronger and ectopic GUS staining in young floral organ primordia and floral meristems (Fig. 3C,D). In *tso1-1* plants with a strong phenotype, including meristem fasciation and a lack of floral organ differentiation, strong, punctate and ectopic staining were observed in young floral meristems (Fig. 3E,F). As *tso1-1* mutants do not form well differentiated stamen or carpels, we do not see strong blue staining in gynoecium or anthers.

Although *tso1-1* mutant inflorescences showed an increased and ectopic CYCA3;4-GUS protein accumulation, we did not observe a corresponding increase in *CYCA3;4* transcript levels in *tso1-1* SAM (Fig. S3), suggesting that the *tso1-1* mutation may affect CYCA3;4 protein levels indirectly. Nevertheless, the resulting increased and ectopic CYCA3;4 protein activity may excessively promote cell proliferation in *tso1-1* mutant inflorescences. A second and distinct interpretation is that the increased and ectopic CYCA3;4 protein accumulation could be a consequence of *tso1-1* mutant cells that are unable to complete the cell cycle and arrest at cell cycle phases that express CYCA3;4 proteins. In this second scenario, stronger CYCA3;4 protein accumulation could be simply a byproduct of the cell division defect of *tso1-1*.

We also compared the *CYCA3;4* reporter expression in the roots. Consistent with previous published data (Willems et al., 2020), the CYCA3;4-GUS fusion proteins are located in the meristematic zone and the transition zone in all cell layers (Fig. 3G). In the elongation zone, CYCA3;4-GUS fusion is restricted in the stele. Similar to the wild type, the CYCA3;4-GUS fusion proteins are also restricted to the same tissues in *tso1-1* roots (Fig. 3G). However, the meristem zone is compressed in *tso1-1* root. Furthermore, whereas the CYCA3;4-GUS proteins are slightly more abundant near the transition zone in the wild-type root (bracketed area in the wild-type root, Fig. 3G), CYCA3;4-GUS seems to be more evenly distributed throughout the meristematic zone and lacks a strong staining band at the transition zone (see transition zone marked by arrows, Fig. 3G). In summary, *TSO1* does not seem to repress the CYCA3;4-GUS in the root, but may affect its spatial distribution.

Overexpression of *CYCA3;4* weakly enhances the *tso1-3* fertility defect

If the elevated *CYCA3;4* activity in *tso1-1* is responsible for some of the *tso1-1* mutant phenotypes, overexpressing *CYCA3;4* in the weak *tso1-3* mutants may enhance the *tso1-3* phenotype. To test this, *pUBQ10::CYCA3;4* was introduced into *tso1-3*/+ plants and RT-qPCR showed 7- to 16-fold higher expression of *CYCA3;4* in three different *pUBQ10::CYCA3;4* transgenic lines (Fig. S4). *tso1-3*

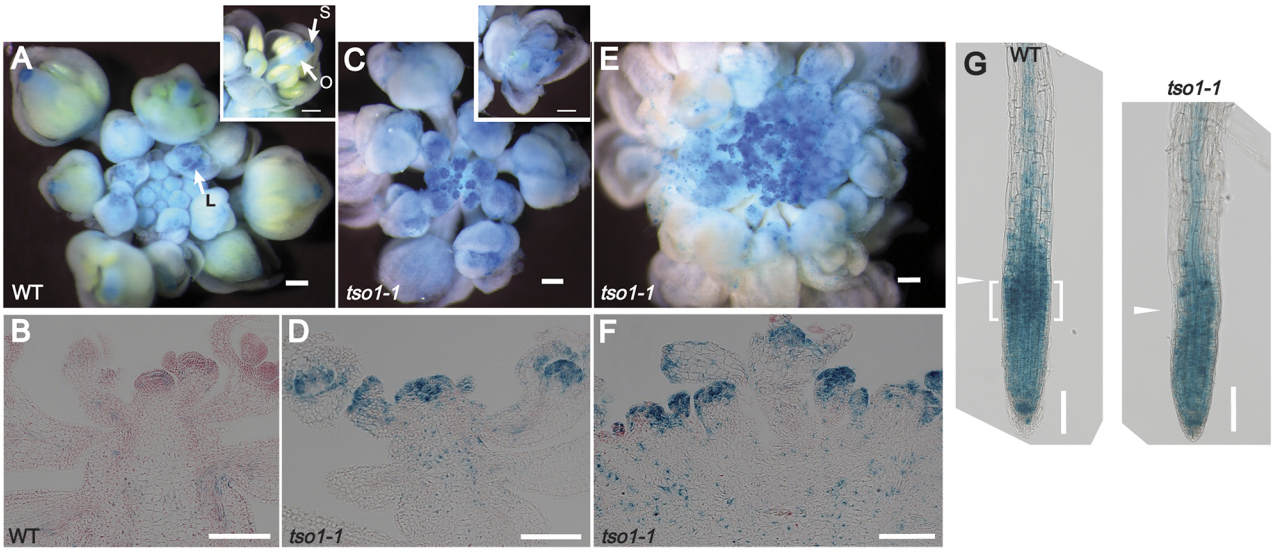

Fig. 3. CYCA3;4 translational reporter expression in wild type and *tso1-1*. (A) The CYCA3;4-GUS translational reporter expression (blue) in an inflorescence of a wild-type (L*er*) transgenic plant. Inset shows a stage 11 flower. Arrows indicate the locule (L) of an anther, stigma (S) and ovules (O). (B) A longitudinal section of the wild-type inflorescence in A. Eosin Y counterstains the tissues in pink. (C) The CYCA3;4-GUS translational reporter expression in the inflorescence of a *tso1-1* transgenic plant. Inset is a stage 11 flower. (D) A longitudinal section of the *tso1-1* inflorescence in C with strong and patchy GUS staining throughout the young floral meristems and organ primordia. (E) CYCA3;4-GUS expression in an fasciated *tso1-1* inflorescence. Significantly more young floral meristems are formed, and all of them are strongly blue. (F) A longitudinal section of the same *tso1-1* inflorescence shown in E. (G) CYCA3;4-GUS expression in the root tip of wild type (L*er*) and *tso1-1* seedlings at 5 days post germination (DPG). Arrowheads indicate the upper boundary of the root apical meristem (RAM) and the brackets indicate a stronger GUS staining band at the most distal region of the RAM. Scale bars: 200 µm in A, C and E; 100 µm in B, D, F and G.

Development (2023) 150, dev201405. doi:10.1242/dev.201405

plants containing the *pUBQ10::CYCA3;4* transgene showed a higher number of defective carpels than *tso1-3* plants without the transgene (Fig. 4B,C). Two of the three *tso1-3* transgenic lines also made fewer seeds per silique than *tso1-3* (Fig. 4C). Therefore, overexpressing *CYCA3;4* enhances the floral organ defect and the fertility defect of *tso1-3*.

In contrast to *tso1-3* plants, the inflorescences and carpels of wild-type plants with the *pUBQ10::CYCA3;4* transgene exhibited no abnormal phenotype (Fig. 4A). One possible explanation is that other partners of *CYCA3;4*, which might not be mis-expressed in the wild-type background, are needed in order for *pUBQ10::CYCA3;4* to confer a mutant phenotype. One such partner could be *MYB3R1*. Ectopically expressed *MYB3R1* in *tso1-1* has previously been shown to mediate the majority of the *tso1-1* phenotypes (Wang et al., 2018). The ectopically expressed MYB3R1 protein in *tso1-1* could rely on CYCA3;4-mediated phosphorylation to become functional (Fig. 4D).

A proposed model

We propose a model that summarizes previous as well as current findings (Fig. 4D). Specifically, *TSO1* acts transcriptionally to prevent *MYB3R1* expression. In *tso1-1* mutants, *MYB3R1* is over- and constitutively expressed, and the constitutive MYB3R1 activity underlies the *tso1-1* mutant phenotype (Wang et al., 2018). However, in the *tso1-1; cyca3;4* double mutants, the constitutive MYB3R1 activity is reduced or lost due to an absence of CYCA3;4 and/or CDK and hence a loss or reduction of phosphorylation of MYB3R1. This explains why merely overexpressing *CYCA3;4* in wild type was insufficient to induce *tso1*-like phenotype (Fig. 4A). This is also supported by our previous experiment (Wang et al., 2018), when we found phosphorylated serine residues at positions 656 and 709 of MYB3R1 by mining the Arabidopsis Protein Phosphorylation Site Database (PhosPhAt 4.0). Phosphomimics on these two residues showed that MYB3R1(S656D) was able to enhance the *tso1-3* fertility defect (Wang et al., 2018). Furthermore, S656, which is immediately followed by PVLDRR, matches the minimal CDK consensus phosphorylation site (S/T-P) (Örd et al., 2019), supporting the possibility that MYB3R1-S656 is likely phosphorylated by a CDK. Accordingly, CDKA;1 could be a partner of CYCA3;4 based on early research showing that the *Arabidopsis* CYCA3;4 can bind CDKA;1 (Van Leene et al., 2010).

In our proposed model, *TSO1* is shown to repress *CYCA3;4* indirectly. This is because *TSO1* encodes a transcriptional regulator and its impact on CYCA3;4 protein is likely to be indirect. Future molecular, genetic and biochemical experiments will be necessary to test different aspects of our proposed model.

MATERIALS AND METHODS

Plant materials and growth conditions

Plants were grown on soil (Sungrow) under a 16 h light/8 h dark cycle at 20°C. All mutants used are in Landsberg *erecta* (L*er*) background. *tso1-1*, *tso1-3* and plants heterozygous for *tso1-1* or *tso1-3* (*tso1-1 +/+ sup-5* and *tso1-3 +/+sup-5*) have been described previously (Hauser et al., 1998; Liu et al., 1997; Sijacic et al., 2011; Wang et al., 2018). *cyca3;4-4* (A144) was

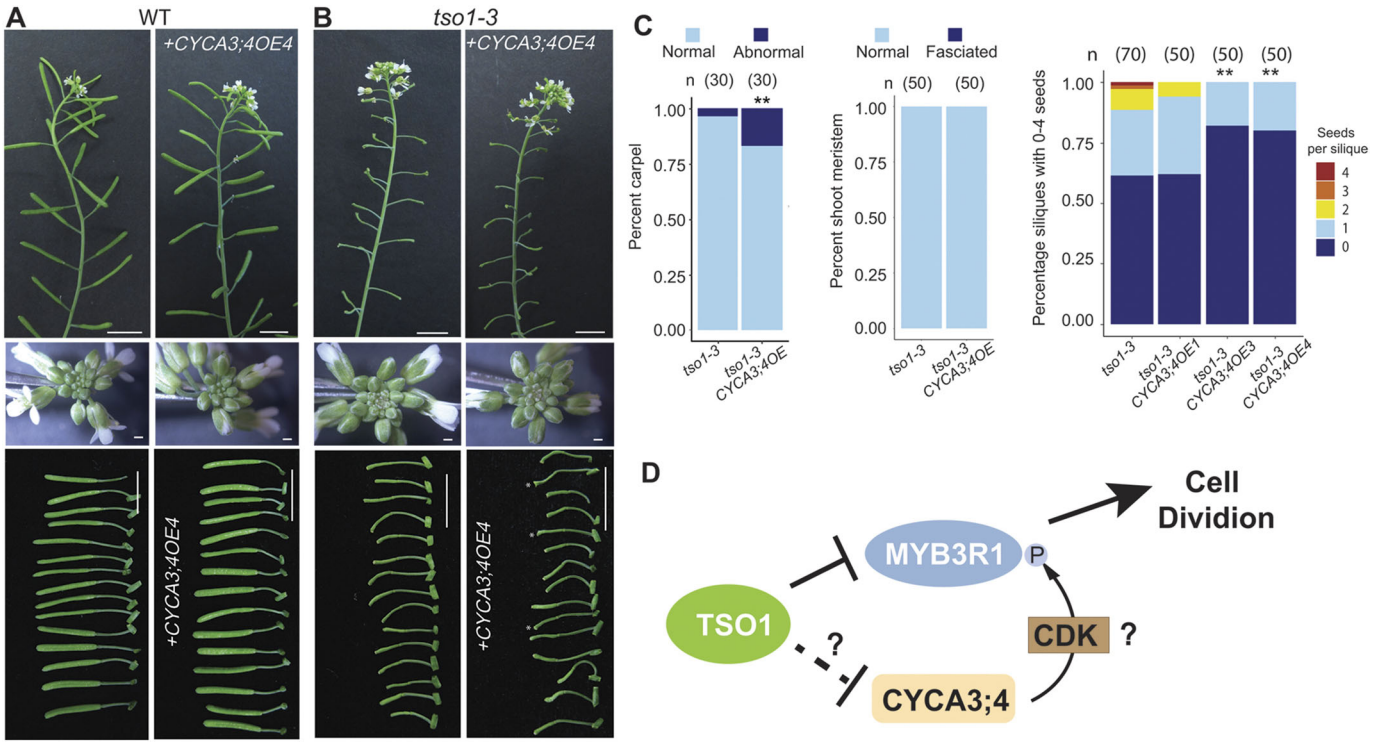

Fig. 4. Overexpression of *CYCA3;4* enhances *tso1-3* fertility defects. (A) Wild-type (L*er*) plants with or without the *CYCA3;4* overexpressing transgene. Transgenic line *CYCA3;4OE4* is shown. (B) *tso1-3* plants with or without the *CYCA3;4* overexpressing transgene. Transgenic line *CYCA3;4OE4* is shown. Abnormal carpels are marked with asterisks. Scale bars: 1 cm (top and bottom rows); 500 µm (middle row). (C) Quantification of carpel, meristem and silique phenotypes in *tso1-3; CYCA3;4* overexpressing transgenic lines in comparison with *tso1-3*. Numbers in parentheses indicate the number of carpels, shoots and siliques that were scored. The carpel graph is from *CYCA3;4OE3* and *CYCA3;4OE4* transgenic lines combined; the meristem graph is derived from *CYCA3;4OE4*. $^{**}P<0.05$ (unpaired, two-tailed *t*-test for carpel and one-way ANOVA and Tukey's test for silique). (D) A proposed *TSO1* regulatory network, where *TSO1* limits cell division in the SAM by repressing the expression of *MYB3R1* and CYCA3;4 protein. At the same time, CYCA3;4, together with CDK, may activate MYB3R1 through phosphorylation. The dotted line implies indirect regulation. The question marks indicate the need for experimental support. Arrows indicate positive regulation; bars indicate negative regulation.

Development (2023) 150, dev201405. doi:10.1242/dev.201405

isolated from an EMS mutagenesis screen of *tso1-1; 35S::TSO1-GR* (Wang et al., 2018).

Constructs and transformation

All constructs were transformed through floral dip using *Agrobacterium* strain GV3101. All sequences were cloned from L*er*. All relevant primers are listed in Table S1.

For the complementation test construct, the genomic sequence of *CYCA3;4* (from the start of the 5′UTR to the end of the 3′UTR plus ∼1.4 kb upstream of the 5′UTR) was PCR amplified with primers (Table S1), cloned into pCR8/GW/TOPO and LR-recombined into pMDC99 (Curtis and Grossniklaus, 2003).

For the CRISPR/Cas9 construct targeting *CYCA3;4*, the crRNA was designed using the website crispr.dbcls.jp/. Two 19 nucleotide guide sequences (Table S1) were chosen as they had no off-target sites. crRNA1 and crRNA2, respectively, target the first few nucleotides and the last few nucleotides of the first exon. To introduce the two crRNAs into the pHEE401E vector (Wang et al., 2015), cloning PCR was carried out using the pCBT-DT1T2 vector as the template and the PCR product containing the two crRNAs was introduced into pHEE401E via Gibson assembly (Gibson et al., 2009). The construct was transformed into *tso1-1; 35S::TSO1-GR* plants. Only crRNA2 was able to generate successful knockout of *CYCA3;4*. No dexamethasone (DEX) was applied when analyzing the phenotype of the transgenic plants.

A 1.4 kb promoter sequence of *CYCA3;4* plus the genomic sequence of *CYCA3;4* (from the start of 5′UTR to the end of the coding region) were cloned into pCR8/GW/TOPO and recombined into pMDC162 (Curtis and Grossniklaus, 2003) to make the *pCYCA3;4::CYCA3;4-GUS* translational fusion. The construct was transformed into *tso1-1 +/+ sup-5* plants. Seven independent transgenic lines were analyzed. GUS expression pattern was compared between wild-type and *tso1-1* T2 sibling plants derived from the same T_1 parent (*tso1-1 +/+ sup5*).

To overexpress *CYCA3;4*, the *Arabidopsis UBQ10* promoter was cloned from the JH23 vector (Zhou et al., 2021) and used to drive full-length cDNA of *CYCA3;4* (*pUBQ10::CYCA3;4*). *pUBQ10::CYCA3;4* was first cloned into pCR8/GW/TOPO by Gibson assembly and LR recombined into pEarleyGate301 (Earley et al., 2006). *pUBQ10::CYCA3;4* was introduced into agrobacterium GV3101 and used to floral dip *tso1-3 +/+ sup-5* plants. T_2 plants from three independent transgenic lines, 1, 3 and 4, were further analyzed and ∼11 plants per line were scored for phenotypes.

Mapping by sequencing

The mapping population was created by crossing *A144* (in the *tso1-1; 35S::TSO1-GR* background) with the parent plant (+/+, *tso1-1; 35S::TSO1-GR*). Leaf tissues were collected and pooled from 34 suppressed F2 plants and 50 unsuppressed F2 plants, respectively. Genomic DNAs were extracted using the NucleoSpin Plant II Midi Kit (Macherey-Nagel) and then sent for Illumina sequencing (PE-150). The sequencing depth of the suppressed plants was 202 folds. The sequencing depth of the unsuppressed group was 95 folds. The SIMPLE pipeline (Wachsman et al., 2017) was employed for mapping A144 with default settings.

Root assay

The seeds were sterilized with 70% ethanol and 10% bleach, and then kept in water at 4°C in the dark for 2 days, after which the seeds were planted on ½ MS (RPI) medium and allowed to germinate under dim light environment for 2 days. Once germinated, they were transferred to the growth chamber. Five days post-germination (DPG) roots were used for quantification.

GUS staining and sectioning

Inflorescences or 5 DPG seedlings were soaked in 90% acetone for 20 min at room temperature, followed by three washes of staining buffer [0.2% Triton X-100, 50 mM NaHPO4 Buffer (pH 7.2), 2 mM potassium ferrocyanide, 2 mM potassium ferricyanide]. They were then stained in a buffer with 2 mM X-Gluc for 3 to 3.5 h. Tissues were cleared with an ethanol series (20%, 35% and 50%) and then stored in 70% ethanol at 4°C before imaging. Subsequently, tissues were embedded and sectioned based on a published protocol (Hollender et al., 2012). Imaging was performed with Zeiss LSM980 and Zeiss Stemi SV 6.

Sample collection, RNA extraction and RT-qPCR

For *tso1-3* and *pUBQ10::CYCA3;4* individual transgenic lines, the whole inflorescence (three inflorescences per biological replicate, two biological replicates per genotype) were collected. For wild type (L-*er*), *tso1-1* and *tso1-1; myb3r1-9* (both *tso1-1* and *tso1-1; myb3r1-9* possess *35S::TSO1-GR* but no DEX treatment), SAMs were dissected and pooled (15-25 SAMs per biological replicate and four biological replicates per genotype).

RNA was extracted with the RNeasy Mini Kit (Qiagen) and cleaned with DNase I or ezDNase (Invitrogen). cDNAs were synthesized using RevertAid First Strand cDNA Synthesis Kit (Thermo Fisher Scientific) or SuperScript IV VILO Master Mix (Invitrogen). RT-qPCR experiments were performed on the Bio-Rad CFX 96 machine with PowerUp SYBR Green Master Mix (Thermo Fisher Scientific). Each biological replicate was analyzed in three technical replicates. The *TIP41* (*AT4G34270*) gene was the internal control for RT-qPCR of *CYCA3;4* overexpressing lines. The *PP2AA3* (*AT1G13320*) gene was used as the internal control for all other RT-qPCR. Primers are provided in Table S1.

Acknowledgements

We thank Dr. Umeda for their collaborative efforts, Amy Beavan at the Department of Cell Biology and Molecular Genetics Imaging Core for assistance with the Zeiss LSM980, and Dirk Joldersma for critical reading of the manuscript. Some of the text and figures in this paper formed part of F.W.'s PhD thesis in the Department of Cell Biology and Molecular Genetics at the University of Maryland in 2022.

Competing interests

The authors declare no competing or financial interests.

Author contributions

Conceptualization: F.W., W.W., Z.L.; Investigation: F.W., W.W.; Writing - original draft: F.W.; Writing - review & editing: F.W., Z.L.; Supervision: Z.L.; Funding acquisition: F.W., Z.L.

Funding

This work was supported by a Dean's fellowship from the University of Maryland and by an Ann G. Wylie Dissertation Fellowship to F.W. The work was previously supported by the National Science Foundation (MCB0951460 to Z.L.).

Data availability

All relevant data can be found within the article and its supplementary information.

Peer review history

The peer review history is available online at https://journals.biologists.com/dev/lookup/doi/10.1242/dev.201405.reviewer-comments.pdf

References

Andersen, S. U., Algreen-Petersen, R. G., Hoedl, M., Jurkiewicz, A., Cvitanich, C., Braunschweig, U., Schauser, L., Oh, S.-A., Twell, D. and Jensen, E. Ø. (2007). The conserved cysteine-rich domain of a tesmin/TSO1-like protein binds zinc in vitro and TSO1 is required for both male and female fertility in Arabidopsis thaliana. *J. Exp. Bot.* **58**, 3657-3670. doi:10.1093/jxb/erm215

Bulankova, P., Akimcheva, S., Fellner, N. and Riha, K. (2013). Identification of Arabidopsis meiotic cyclins reveals functional diversification among plant cyclin genes. *PLoS Genet.* **9**, e1003508. doi:10.1371/journal.pgen.1003508

Curtis, M. D. and Grossniklaus, U. (2003). A gateway cloning vector set for high-throughput functional analysis of genes in planta. *Plant Physiol.* **133**, 462-469. doi:10.1104/pp.103.027979

Earley, K. W., Haag, J. R., Pontes, O., Opper, K., Juehne, T., Song, K. and Pikaard, C. S. (2006). Gateway-compatible vectors for plant functional genomics and proteomics. *Plant J.* **45**, 616-629. doi:10.1111/j.1365-313X.2005.02617.x

Fischer, M. and Müller, G. A. (2017). Cell cycle transcription control: DREAM/MuvB and RB-E2F complexes. *Crit. Rev. Biochem. Mol. Biol.* **52**, 638-662. doi:10.1080/10409238.2017.1360836

Gibson, D. G., Young, L., Chuang, R.-Y., Venter, J. C., Hutchison, C. A. and Smith, H. O. (2009). Enzymatic assembly of DNA molecules up to several hundred kilobases. *Nat. Methods* **6**, 343-345. doi:10.1038/nmeth.1318

Hauser, B. A., Villanueva, J. M. and Gasser, C. S. (1998). Arabidopsis TSO1 regulates directional processes in cells during floral organogenesis. *Genetics* **150**, 411-423. doi:10.1093/genetics/150.1.411

Hauser, B. A., He, J. Q., Park, S. O. and Gasser, C. S. (2000). TSO1 is a novel protein that modulates cytokinesis and cell expansion in Arabidopsis. *Development* **127**, 2219-2226. doi:10.1242/dev.127.10.2219

Hollender, C. A., Geretz, A. C., Slovin, J. P. and Liu, Z. (2012). Flower and early fruit development in a diploid strawberry, Fragaria vesca. *Planta* **235**, 1123-1139. doi:10.1007/s00425-011-1562-1

Kobayashi, K., Suzuki, T., Iwata, E., Nakamichi, N., Suzuki, T., Chen, P., Ohtani, M., Ishida, T., Hosoya, H., Müller, S. et al. (2015). Transcriptional repression by MYB3R proteins regulates plant organ growth. *EMBO J.* **34**, 1992-2007. doi:10.15252/embj.201490899

Lang, L., Pettkó-Szandtner, A., Elbaşı, H. T., Takatsuka, H., Nomoto, Y., Zaki, A., Dorokhov, S., Jaeger, G. D., Eeckhout, D., Ito, M. et al. (2021). The DREAM complex represses growth in response to DNA damage in Arabidopsis. *Life Sci. Alliance* **4**, e202101141. doi:10.26508/lsa.202101141

Liu, Z., Running, M. P. and Meyerowitz, E. M. (1997). TSO1 functions in cell division during Arabidopsis flower development. *Development* **124**, 665-672. doi:10.1242/dev.124.3.665

Menges, M., De Jager, S. M., Gruissem, W. and Murray, J. A. H. (2005). Global analysis of the core cell cycle regulators of Arabidopsis identifies novel genes, reveals multiple and highly specific profiles of expression and provides a coherent model for plant cell cycle control. *Plant J.* **41**, 546-566. doi:10.1111/j.1365-313X.2004.02319.x

Musa, J., Aynaud, M.-M., Mirabeau, O., Delattre, O. and Grünewald, T. G. (2017). MYBL2 (B-Myb): a central regulator of cell proliferation, cell survival and differentiation involved in tumorigenesis. *Cell Death Dis.* **8**, e2895. doi:10.1038/cddis.2017.244

Ning, Y.-Q., Liu, N., Lan, K.-K., Su, Y.-N., Li, L., Chen, S. and He, X.-J. (2020). DREAM complex suppresses DNA methylation maintenance genes and precludes DNA hypermethylation. *Nat. Plants* **6**, 942-956. doi:10.1038/s41477-020-0710-7

Örd, M., Möll, K., Agerova, A., Kivi, R., Faustova, I., Venta, R., Valk, E. and Loog, M. (2019). Multisite phosphorylation code of CDK. *Nat. Struct. Mol. Biol.* **26**, 649-658. doi:10.1038/s41594-019-0256-4

Sadasivam, S. and DeCaprio, J. A. (2013). The DREAM complex: master coordinator of cell cycle-dependent gene expression. *Nat. Rev. Cancer* **13**, 585-595. doi:10.1038/nrc3556

Sijacic, P., Wang, W. and Liu, Z. (2011). Recessive Antimorphic Alleles Overcome Functionally Redundant Loci to Reveal TSO1 Function in Arabidopsis Flowers and Meristems. *PLoS Genet.* **7**, e1002352. doi:10.1371/journal.pgen.1002352

Simmons, A. R., Davies, K. A., Wang, W., Liu, Z. and Bergmann, D. C. (2019). SOL1 and SOL2 regulate fate transition and cell divisions in the Arabidopsis stomatal lineage. *Development* **146**, dev171066. doi:10.1242/dev.171066

Song, J. Y., Leung, T., Ehler, L. K., Wang, C. and Liu, Z. (2000). Regulation of meristem organization and cell division by TSO1, an Arabidopsis gene with cysteine-rich repeats. *Development* **127**, 2207-2217. doi:10.1242/dev.127.10.2207

Takahashi, I., Kojima, S., Sakaguchi, N., Umeda-Hara, C. and Umeda, M. (2010). Two Arabidopsis cyclin A3s possess G1 cyclin-like features. *Plant Cell Rep.* **29**, 307-315. doi:10.1007/s00299-010-0817-9

Van Leene, J., Hollunder, J., Eeckhout, D., Persiau, G., Van De Slijke, E., Stals, H., Van Isterdael, G., Verkest, A., Neirynck, S., Buffel, Y. et al. (2010). Targeted interactomics reveals a complex core cell cycle machinery in Arabidopsis thaliana. *Mol. Syst. Biol.* **6**, 397. doi:10.1038/msb.2010.53

Wachsman, G., Modliszewski, J. L., Valdes, M. and Benfey, P. N. (2017). A SIMPLE pipeline for mapping point mutations. *Plant Physiol.* **174**, 1307-1313. doi:10.1104/pp.17.00415

Wang, Z.-P., Xing, H.-L., Dong, L., Zhang, H.-Y., Han, C.-Y., Wang, X.-C. and Chen, Q.-J. (2015). Egg cell-specific promoter-controlled CRISPR/Cas9 efficiently generates homozygous mutants for multiple target genes in Arabidopsis in a single generation. *Genome Biol.* **16**, 144. doi:10.1186/s13059-015-0715-0

Wang, W., Sijacic, P., Xu, P., Lian, H. and Liu, Z. (2018). Arabidopsis TSO1 and MYB3R1 form a regulatory module to coordinate cell proliferation with differentiation in shoot and root. *Proc. Natl. Acad. Sci. USA* **115**, E3045-E3054.

Willems, A., Heyman, J., Eekhout, T., Achon, I., Pedroza-Garcia, J. A., Zhu, T., Li, L., Vercauteren, I., Daele, V. d., van de Cotte, H. (2020). The cyclin CYCA3;4 is a postprophase target of the APC/CCCS52A2 E3-ligase controlling formative cell divisions in Arabidopsis. *Plant Cell* **32**, 2979-2996. doi:10.1105/tpc.20.00208

Wu, N., Jia, D., Bates, B., Basom, R., Eberhart, C. G. and MacPherson, D. (2017). A mouse model of MYCN-driven retinoblastoma reveals MYCN-independent tumor reemergence. *J. Clin. Invest.* **127**, 888-898. doi:10.1172/JCI88508

Yu, Y., Steinmetz, A., Meyer, D., Brown, S. and Shen, W.-H. (2003). The tobacco a-type cyclin, Nicta;CYCA3;2, at the nexus of cell division and differentiation. *Plant Cell* **15**, 2763-2777. doi:10.1105/tpc.015990

Zhou, J., Sittmann, J., Guo, L., Xiao, Y., Huang, X., Pulapaka, A. and Liu, Z. (2021). Gibberellin and auxin signaling genes RGA1 and ARF8 repress accessory fruit initiation in diploid strawberry. *Plant Physiol.* **185**, 1059-1075. doi:10.1093/plphys/kiaa087

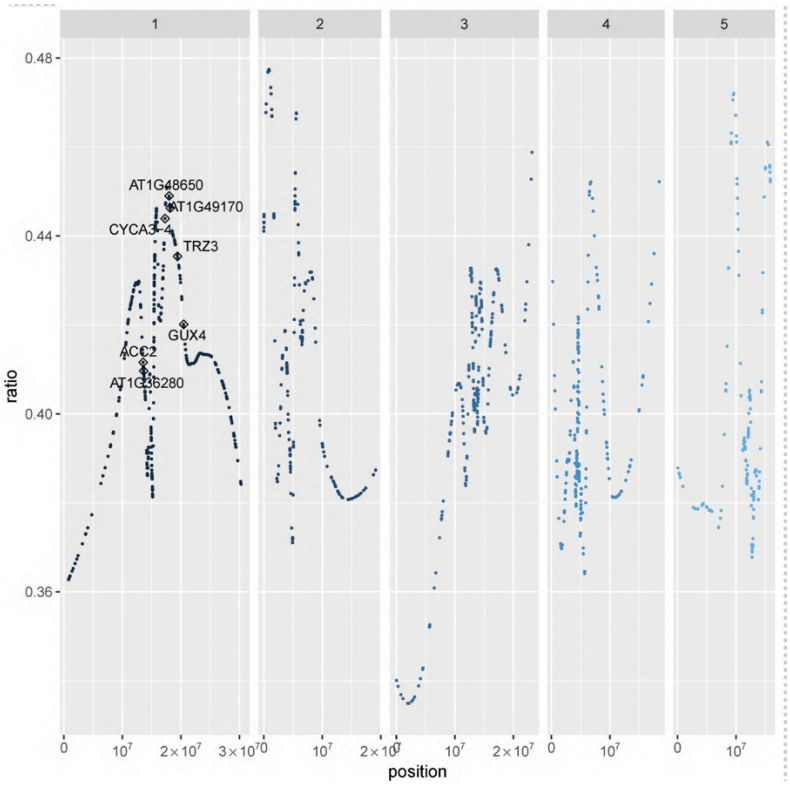

Fig. S1. The Mapping-by-sequencing result showing *CYCA3;4* the best candidate for *A144*. An output plot from the SIMPLE pipeline (Wachsman et al., 2017) showing the allele frequency comparison between the unsuppressed and suppressed plants. *CYCA3;4* (AT1G47230) is located at the peak on Chromosome 1.

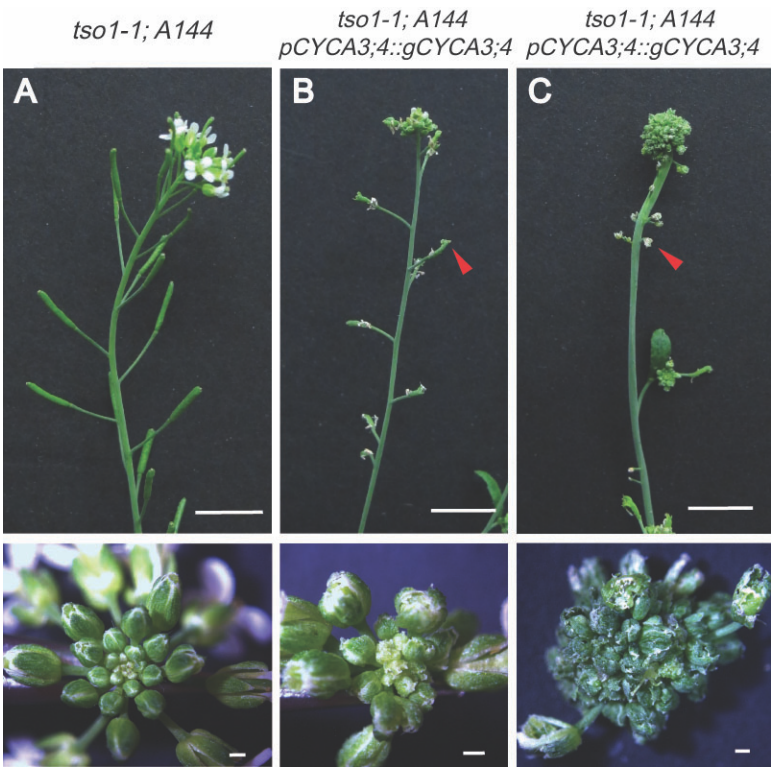

Fig. S2. Complementation test confirming *CYCA3;4* as *A144*.

(A). Top panel shows a *tso1-1; A144* shoot with a normal inflorescence and fertile siliques. Bottom panel shows a top view of a wild type-like SAM in *tso1-1; A144*.

(B)-(C).Two independent transgenic lines showing a loss of suppression due to their harboring the g*CYCA3;4* transgene. Note the sterile carpels (red arrowheads). The bottom panel shows top view of a SAM and reveals a severely fasciated SAM in C. Scale bars: 1cm in the top row and 500µm in the bottom row.

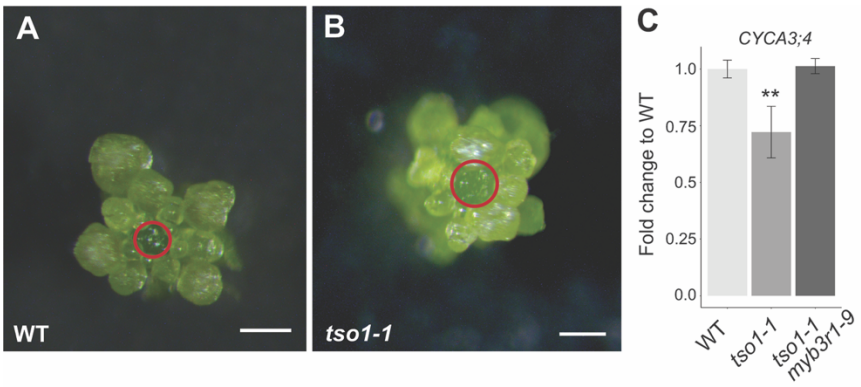

Fig. S3. RT-qPCR of *CYCA3*;4 in *tso1-1* mutant shoot apical meristems.
(A)-(B): Microphotographs of dissected shoot apical meristem. The red circles highlight the meristem tissue isolated for RT-qPCR. (C) RT-qPCR results of *CYCA3;4* in respective genotypes. The fold change relative to WT (Y-axis) was calculated based on four biological replicates, each with three technical replicates. Significant difference (two-tailed Student's *t*-test) is indicated by ** ($P < 0.05$) and *** ($P<0.01$). Error bars indicate standard deviation of the mean. Scale bars: 200μm in A,B.

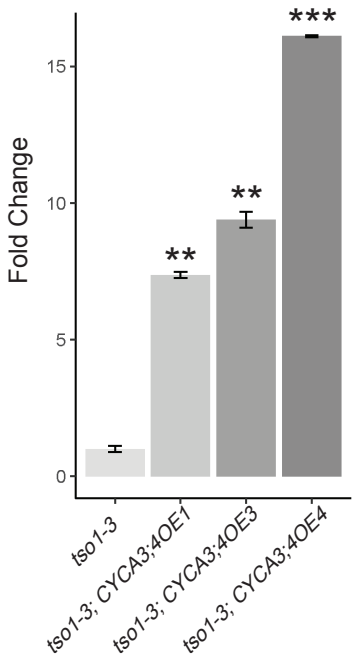

Fig. S4. *CYCA3;4* expression in the three *CYCA3;4OE* transgenic lines.
RT-qPCR results showing the *CYCA3;4* transcript levels in *CYCA3;4OE* lines relative to *tso1-3*. Significant difference from *tso1-3* (one-way ANOVA and Tukey's test) is indicated by ** ($P < 0.05$) or *** ($P<0.01$). Error bars indicate standard deviation of the mean.

Table S1. Primer information

Primer Name	Sequence (5'-3')	Notes
CYCA3;4 complement F	GTACAAAAAAGCAGGCTCCGtcagaaccaatctttcatttcc	Cloning for the complementation construct. Forward primer also for making the translational reporter
CYCA3;4 complement R	TGTACAAGAAAGCTGGGTCGtagctgcacaaaaataactgcc	
crRNA1	GGAGAATCAGAACTGTGCGAGG	CRISPR sgRNA1 for CYCA3;4
crRNA2	GCTTATCTCCGTGAAATGGAGg	CRISPR sgRNA2 for CYCA3;4
CYCA3;4 CR F	TAGAGTCGAAGTAGTGATTGGGAGAATCAGAACTGTGCGGTTTTAGAGCTAGAAATAGC	Primers for cloning crRNAs into destination vector
CYCA3;4 CR R	GCTATTTCTAGCTCTAAAACCCATTTCACGGAGATAAGCAATCTCTTAGTCGACTCTAC	
CYCA3;4 genotyping F	ATGGCGGAGAATCAGAACTGTGC	Primers for identifying CRISPR-induced mutation
CYCA3;4 genotyping R	AACCGCTCTCATGTGTGGAGTT	
CYCA3;4 GUS R	TGTACAAGAAAGCTGGGTCGCGCCATTCCTCTAATGGTAA	Reverse primer for cloning the translational reporter
pUBQ F	AGGCTCCGAATTCGGCGCGCCCATGCATATGAGTCTAGCTC	Primers for cloning *UBQ10* promoter
pUBQ R	TGATTCTCCGCCATGGATCCTTGTAATTGTAAATAGTAATTGTAATG	
CYCA3;4 CDS F	ATTTACAATTACAAGGATCCATGGCGGAGAATCAGAACTG	Primers for cloning CDS of *CYCA3;4*
CYCA3;4 CDS R	GCTGGGTCGAATTCCTCGAGCGCCATTCCTCTAATGGTAA	
CYCA3;4 qPCR F	GGGAGTTTCTGCAATGCTTATT	Primers for RT-qPCR of *CYCA3;4*
CYCA3;4 qPCR R	CAAGAAGTATATCCGCCTCCAT	
TIP41 qPCR F	TTTTGGCGAGAATGCATTAGTC	Primers for RT-qPCR control gene *TIP41*
TIP41 qPCR R	TTGCTCCTGAATTTCCATTGTG	
PP2AA3 qPCR F	GCATATGCTCGTCTACTTTGTG	Primers for RT-qPCR control gene *PP2AA3*
PP2AA3 qPCR R	AGTTCAGGGTTTAAAATGCGAC	

Reference

Wachsman, G., Modliszewski, J. L., Valdes, M. and Benfey, P. N. (2017). A SIMPLE Pipeline for Mapping Point Mutations. *Plant Physiology* **174**, 1307–1313.